ACS OMEGA

http://pubs.acs.org/journal/acsodf

Article

Zein-Based Nanomedicines for Synergistic Chemodynamic/Photodynamic Therapy

Xiang Li, Yupeng Wang, Qiankun Shi, Nuo Zhen, Jin Xue, Jingsheng Liu, Dongfang Zhou,* and Hao Zhang*

Cite This: *ACS Omega* 2022, 7, 29256−29265

Read Online

ACCESS | Metrics & More | Article Recommendations | Supporting Information

ABSTRACT: Current cancer treatment is not only limited to monotherapy but is also influenced by limited drug delivery options. Combined chemokinetic-photokinetic therapy has great promise in enhancing anticancer effects. Meanwhile, zein has superior self-assembly properties and can be loaded with photosensitizers. Herein, the targeted multifunctional nanoparticles based on zein/hyaluronate acid (HA)/tannin (TA)/Cu^{2+} loaded with IR780 (ZHTC@IR780) are constructed for synergetic cancer therapy by chemo-dynamic therapy (CDT) and photodynamic therapy (PDT). There is experimental proof that ZHTC@IR780 nanoparticles (NPs) can relieve the tumor hypoxic microenvironment by catalytic decomposition of endogenous H_2O_2 to O_2 and further react with O_2 to produce toxic $^1O_2$ with 808 nm laser irradiation. The glutathione oxidase-like effects of ZHTC@IR780 NPs can generate Fenton-like Cu^+ ions and deplete GSH for efficient hydroxyl radical ($^\bullet$OH) production. In addition, CDT combined with PDT enhances the antitumor effect. Photodynamic therapy can cause immunogenic cell death, increase calreticulin eversion, release histone with high mobility, and promote apoptosis of tumor cells.

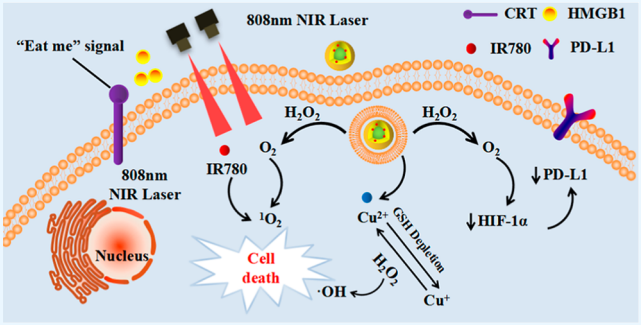

INTRODUCTION

Cancer is a common disease that poses a serious risk to human health and has become a leading cause of death worldwide. At present, the main clinical treatments for cancer are surgical resection, chemotherapy, and radiation therapy.[1−4] The tumor microenvironment (TME) of solid tumors with severe hypoxia, high H_2O_2 levels, and glutathione (GSH) overexpression promotes tumor proliferation and metastasis.[5,6] Therefore, it is difficult to completely cure tumors with monotherapy, and combined therapy with adjustment of TME is of great significance for ablating primary tumors and preventing tumor metastasis.[7−9] Among these, comprehensive treatments such as photodynamic therapy (PDT) and chemical dynamic therapy (CDT) utilize specific intracellular chemical reactions to produce cytotoxic reactive oxygen species (ROS), including singlet oxygen ($^1O_2$), hydroxyl radicals ($^\bullet$OH) and superoxide anion ($^\bullet O_2^-$). Although photodynamic therapy has the advantages of light pain, small side effects, and low systemic toxicity, the active oxygen generation efficiency of photodynamic therapy is low due to the hypoxic TME and rapid energy attenuation.[10,11] In recent studies, combined therapies such as PDT/photothermal therapy (PTT), PDT/chemotherapy, and PDT/immunotherapy have been used to overcome monotherapy's insufficient tumor suppression effect.[1,6,7,12−19] From the abovementioned, we know that under the tumor microenvironment, Fenton or Fenton-like reactions can generate $^\bullet$OH and O_2 at the same time, which indicates that CDT can improve the hypoxia deficiency in PDT and enhance its therapeutic effects, while UV−vis or near-infrared laser irradiation can increase the efficiency of the Fenton reaction to produce $^\bullet$OH and improve the antitumor effects of CDT.[20−22] Jia et al., for example, developed a smart TME responsive nanocatalyst by employing Fe−Mn layered double hydroxides (FeMn-LDH) as an efficient photothermal nanocarrier to load mesoporous silica and Ce6 covalently coated upconversion nanoparticles (UCSP) for multimodal imaging and directed therapy.[16] This work achieved excellent oxygen-elevated PDT, enhanced PTT and CDT synergistic therapy, and real-time monitoring of the therapeutic effect.

Nanoparticles are widely used in the development of controlled drug delivery systems as well as in the diagnosis and treatment of cancer due to their good physicochemical and biological properties such as size, hydrophobicity, and surface charge.[23] The smaller size of nanoparticles allows them to be used as carriers of drugs into the body, improving their

Received: June 1, 2022
Accepted: July 21, 2022
Published: August 8, 2022

ACS Publications

© 2022 The Authors. Published by American Chemical Society

https://doi.org/10.1021/acsomega.2c03404
ACS Omega 2022, 7, 29256−29265

bioaccessibility. Protein-based nanomaterials offer advantages such as biodegradability and biocompatibility.[24] Zein is the main storage protein in corn endosperm,[25] and it contains hydrophobic, neutral, and polar amino acids. It is typically only soluble in an aqueous 60−95% ethanol solution.[26] Many researchers have used its poor solubility to induce self-assembly into nanoparticles by antisolvent precipitation and complexation with hydrophilic polysaccharides to improve storage stability in water. Hyaluronic acid is a biocompatible polysaccharide composed of D-glucuronic acid and *N*-acetyl-D-glucosamine, which can form hydrogen bonds in solution and can act as a stabilizer and targeting agent.[27] It has been demonstrated that hyaluronic acid-coated zein core−shell nanoparticles can achieve HNK-targeted delivery to over-expressing 4T1 breast cancer cells, overexpressing CD44 with high encapsulation efficiency, enhanced stability, and slow release properties, making them suitable as an efficient drug delivery system.[28]

As a water-soluble polyphenol widely distributed in the plant kingdom, tannins have a wide range of restorative, therapeutic, and pharmacological properties,[29] and the catechol or gallic acyl groups in their structure can provide chelating sites for metal ions and have a strong chelating effect on them.[30] Also, due to the potential binding sites between tannins and hydrophobic amino acids in zein, such as proline and phenylalanine,[31] recent research has used intermolecular interactions between zein and tannic acid to modify the model protein β-galactosidase and encapsulate it in spore powder outer wall capsules, where stronger binding of zein/TA to the drug improved the protein's sustained delivery.[32] In short, tannins and zein are suitable as efficient and stable composite nanomaterials for drug delivery.

Here, the zein is used as a carrier for the IR780 stretcher. A targeted multifunctional nano-drug ZHTC@IR780 NPs was prepared for the first time, which achieved synergistic cancer therapy by chemodynamic therapy, phototherapy, and immunotherapy (Scheme 1). First, ZHTC@IR780 NPs with catalase-like activity could react with endogenous H_2O_2 to generate O_2 for accelerating $^1O_2$ production under 808 nm laser irradiation. Meanwhile, multivalent elements ($Cu^{1+/2+}$) of ZHTC@IR780 NPs demonstrated superior OH generation ability via Fenton-like reaction to realize CDT and consume overexpressed GSH in TME for modulating the tumor's antioxidant capability via glutathione peroxidase-like activity. The IR780 acts as a significant photosensitizer when stimulated by NIR light and could be activated to produce $^1O_2$ for PDT therapy. Collectively, the ZHTC@IR780 NPs multivalent elements ($Cu^{1+/2+}$) exhibit Fenton-like, glutathione (GSH) peroxidase-like, and catalase-like activity. In addition, the ZHTC@IR780 NPs under 808 nm laser irradiation show remarkable tumor-killing ability by phototherapy due to their excellent photothermal conversion efficiency and cytotoxic super $^1O_2$ generation performance. This work provides an innovative strategy for the synergistic and integrative treatment of cancer, and zein-based nanomedicine drugs may have great potential as a promising candidate for cancer therapeutics.

Scheme 1. Mechanism of Nanoparticles Inducing Tumor Cell Apoptosis

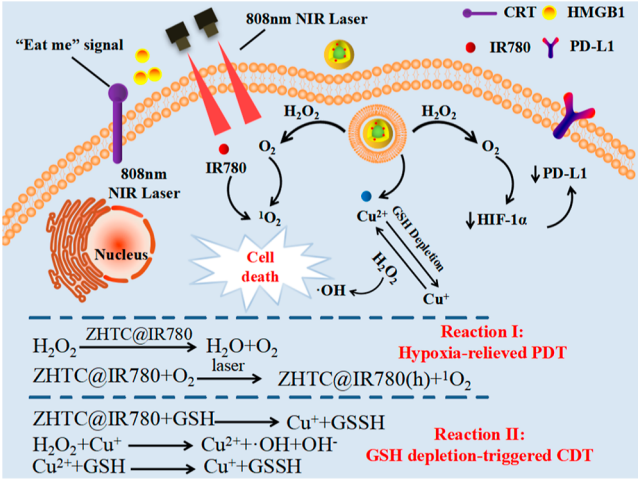

EXPERIMENTAL SECTION

Materials and Method. *Materials.* All reagents and solvents were obtained commercially and used without further purification. Zein (≥98%), sodium hyaluronate (97%), sodium carboxymethyl cellulose (CMC, USP), tannic acid (98%), and IR780 (95%) were obtained from Sigma-Aldrich. Copper chloride dihydrate ($CuCl_2{\cdot}2H_2O$), 1,3 diphenylisobenzofuran (DPBF), and methylene blue trihydrate (MB) were purchased from J&K Chemical Co. The mouse colon cancer cell CT26 was obtained from the Chinese Academy of Sciences' Institute of Biochemistry and Cell Biology and was cultured in DMEM (10% fetal bovine serum; 5% CO_2 at 37 °C). Other chemicals were purchased from Sinopharm Chemical Reagent Co., Ltd., China.

Instrumentation. The morphologies of nanoparticles were obtained by transmission electron microscopy (TEM, JEM1011, Japan). The particle size and zeta potential were performed by the Zetasizer Nano ZS90 system (Malvern, UK). X-ray photoelectron spectroscopy (XPS) spectra were obtained using the Thermo Scientific ESCALAB 250 XI. Real-time measurement of O_2 concentration in a solution was performed by a portable dissolved oxygen meter (JPBJ-608, Rex, INESA Scientific Instruments). The UV−visible absorption was obtained by a UV-1800 spectrophotometer (Shimadzu, Japan). The cell fluorescence imaging experiments were carried out using a confocal laser scanning fluorescence microscope (CLSM, FV1000, Olympus, Japan). The concentration of released Cu of CMSNs and the concentration of Cu in blood samples and tissues were measured by inductively coupled plasma-optical emission spectrometry (ICP-OES, Xseries II, Thermo Scientific, USA). It was used to analyze the targeting ability of Zein-HA-TA-Cu@IR780 nanoparticles.

Synthesis of Zein-HA-TA-Cu@IR780 (ZHTC@IR780) Nanoparticles. The nanoparticle synthesis method was as follows: zein was dissolved in a 90 v/v % aqueous solution of ethanol (zein, 10 mg/mL) and stirred for 2 h to be fully dissolved and then used. The low molecular weight sodium hyaluronate (20 mg) was added to 9 mL of distilled water and then magnetically stirred at room temperature for sufficiently long enough time to dissolve. Then, 2 mg of IR780 was dissolved in 1 mL of dimethyl sulfoxide, and then added to sodium hyaluronate drop by drop, simultaneously with 1 mL of prepared 10 mg/mL zein solution, and magnetically stirred for 5 min. The ethanol was then removed by dialysis for 4 h with a molecular weight cutoff (MWCO) of 3500 Da. After the end of the dialysis, 100 μL of a tannic acid solution (24 mM) was added dropwise, and the mixture was stirred for 10 min; then, 30 μL of a copper chloride dihydrate solution (72 mM) was

https://doi.org/10.1021/acsomega.2c03404
ACS Omega 2022, 7, 29256−29265

added dropwise, and the mixture was further dialyzed for 10 h. The resulting nanomaterial was then stored at 4 °C. The Zein, Zein-HA, Zein-HA-TA-Cu, and Zein-CMC-TA-Cu nanoparticles were used as comparison groups for ZHTC@IR780 nanoparticles. The preparation method is the same as mentioned above.

pH-Responsive Release of Drug-Loaded Nanoparticles IR780 and Cu^{2+} In Vitro. The release of IR780 was performed as follows: at a certain concentration, 2 mL of the prepared drug-laden nanoparticles were transferred to a dialysis bag (with an MWCO of 3500 Da). The bag was tied and submerged in 18 mL of PBS solution in the dialysis solution and placed in a 37 °C shaker at 100 rpm to avoid light. The dialysate was divided into two groups, one with PBS solution at pH 7.4 and the other with PBS solution at pH 5.0. At regular intervals, 2 mL of dialysate was removed, and 2 mL of the corresponding pH of PBS solution was added to the dialysate. The released IR780 content of the removed dialysate was measured by a UV spectrometer and the cumulative IR780 release was calculated.

The Cu^{2+} release operation was performed as mentioned above, and the released Cu^{2+} content of the removed dialysate was determined by ICP-OES, and the cumulative Cu^{2+} release was calculated.

Extracellular Real-time O_2 Concentration Measurement. Under vigorous stirring, 3 mL of ZHTC@IR780 nanoparticles (IR780 2.5 μg/mL) and 100 μL of H_2O_2 (10 mM) were added to 3 mL of water in turn, under vigorous stirring, and the O_2 concentration of the solution was monitored by a portable dissolved oxygen meter in real time.

Singlet Oxygen ($^1O_2$) Detection. Measurement of Singlet Oxygen Generation By using the trapping agent DPBF (Aladdin Regent, Shanghai), which was used to confirm singlet oxygen by detecting its absorption intensity at 421 nm via UV−vis spectroscopy, was used to detect the ZHTC@IR780 nanoparticle-enhanced $^1O_2$ generation in the presence of H_2O_2. Before the detection, the prepared system was irradiated by an 808 nm laser (0.1 W/cm^2) for 5 s. In a typical experiment, DPBF (0.15 mg/mL) in alcohol was added to the ZHTC@IR780 nanoparticles solution (3 mL, IR780 2.5 μg/mL). The solution was saturated with an Ar atmosphere and irradiated with an 808 nm laser (0.1 W/cm^2) for 30 min, and the absorption intensity of DPBF at 421 nm was recorded every 5 s. In the control experiments, the solution was not saturated with the Ar atmosphere. Herein, a hypoxic condition was achieved by Ar blowing into the solution for 30 min before the test.

Evaluation of •OH Production. A classical colorimetric method was used based on the degradation of MB under the oxidative environment. In brief, ZHTC@IR780 was added into an aqueous solution containing H_2O_2 (10 mM) and MB (15 μg mL^{-1}). After incubation at 37 °C for various time intervals, the absorption of the abovementioned solutions at 665 nm was measured to record the degradation of MB.

In Vitro ZHTC@IR780 NPs Assay on GSH Depletion Properties. GSH was detected by DTNB and its UV−vis absorption was measured at 313 nm and 408 nm. The samples were divided into seven groups: DTNB group: 10 μL DTNB (2.5 mg/mL) + 990 μL PBS; ZHTC@IR780 group: 80 μL ZHTC@IR780 (1 mg/mL) + 920 μL PBS; GSH group: 10 μL GSH solution (10 mM) + 990 μL PBS; ZHTC@IR780 + GSH group [80 μL ZHTC@IR780 solution (1 mg/mL) + 10 μL GSH solution (10 mM) + 910 μL PBS]; GSH + DTNB group: 10 μL GSH solution (10 mM) + 10 μL DTNB (2.5 mg/mL) + 980 μL PBS; and ZHTC@IR780 + DTNB group: 80 μL ZHTC@IR780 solution (1 mg/mL) + 10 μL DTNB (2.5 mg/mL) + 910 μL PBS; except for the ZHTC@IR780 + GSH + DTNB group, UV−visible spectra were performed after homogeneous solute mixing for 10 min in all cases. The ZHTC@IR780 + GSH + DTNB group was operated as follows: first GSH and ZHTC@IR780 nanoparticles were reacted for 10 min, and then DTNB solution was added and treated for 10 min, followed by UV−visible spectroscopy.

Cell Experiment. In this experiment, mouse colon cancer cells (CT26) were cultured in the DMEM (GIBCO) medium. The DMEM medium contains 10% fetal bovine serum and 10% penicillin−streptomycin mixture (100×).

Uptake Analysis. The endocytosis of drug-loaded nanoparticles by CT26 cells was observed by a laser confocal scanning microscope (CLSM). The cells were inoculated into a six-well plate and cultured overnight to make them adhere to the wall. Then, CT26 cells were incubated with free small molecules IR780, ZHT@IR780, ZHTC@IR780, and ZCTC@IR780 IR780 (the concentration of IR780 is the same: 1 μg/mL) at 37 °C for 4 h and washed with PBS three times.

The cells were stained with 1 mL of the lysosomal green fluorescent probe (Lyso-Tracker, 50 nM) for 40 min, washed three times with PBS, fixed with 4% paraformaldehyde for 15 min, and washed three times with PBS. Finally, the cells were stained with DAPI for 8 min, washed with PBS three times, and mounted. CLSM was used to observe the intensity and position of fluorescence in cells. DAPI is excited at 405 nm; the lysosomal green fluorescent probe is excited at 488 nm; IR780 is excited at 555 nm.

Determination of Reactive Oxygen Species. The intracellular ROS of each group was detected by the DCF-DA probe. Cells from CT26 cells (1×10^5 cells/well) were inoculated into a six-well plate and cultured overnight to make the cells adhere to the wall. Then CT26 cells were incubated with the medium solution of free small molecules IR780, ZHT@IR780, ZHTC@IR780, and ZCTC@IR780 (IR780 concentration: 1 μg/mL) for 4 h, and the light group was exposed to light (0.1 W/cm^2). After 30 min, the abandoned culture medium was washed with PBS three times, and then, for 20 min, it was incubated with a serum-free medium containing DCF-DA. Among them, in the no-light control group, all operations were the same as in the light group except no light was applied. Finally, we used a laser confocal scanning microscope to observe the production of cellular ROS, which was excited with a 488 nm channel, with green fluorescence indicating ROS production.

In Vitro Cytotoxicity. CT26 cells were seeded in 96-well plates at a density of 1×10^4 cells per well in DMEM (100 μL) containing 10% FBS at 37 °C under a 5% CO_2 humidified atmosphere or in a hypoxic incubator. After 12 h of incubation, the medium was removed, and then, fresh DMEM with 10% FBS was added. IR780, ZH@ IR780, ZHT@ IR780, and ZHTC@ IR780 were used at various final concentrations in DMEM (0.3125, 0.62, 1.25, 2.5, and 5.0 g/mL). IR780 (1.0 mM) was dissolved in a little dimethyl sulfoxide (DMSO) and added to the cell culture medium. To minimize the influence of DMSO, the final DMSO concentration in the medium was controlled to less than 0.1%. After 4 h of incubation, excess unbound materials were washed three times with PBS. The cells were exposed to an 808 nm laser at a power density of 0.1 W/cm^2 for 3 min after adding fresh DMEM into 96-well plates.

https://doi.org/10.1021/acsomega.2c03404
ACS Omega 2022, 7, 29256−29265

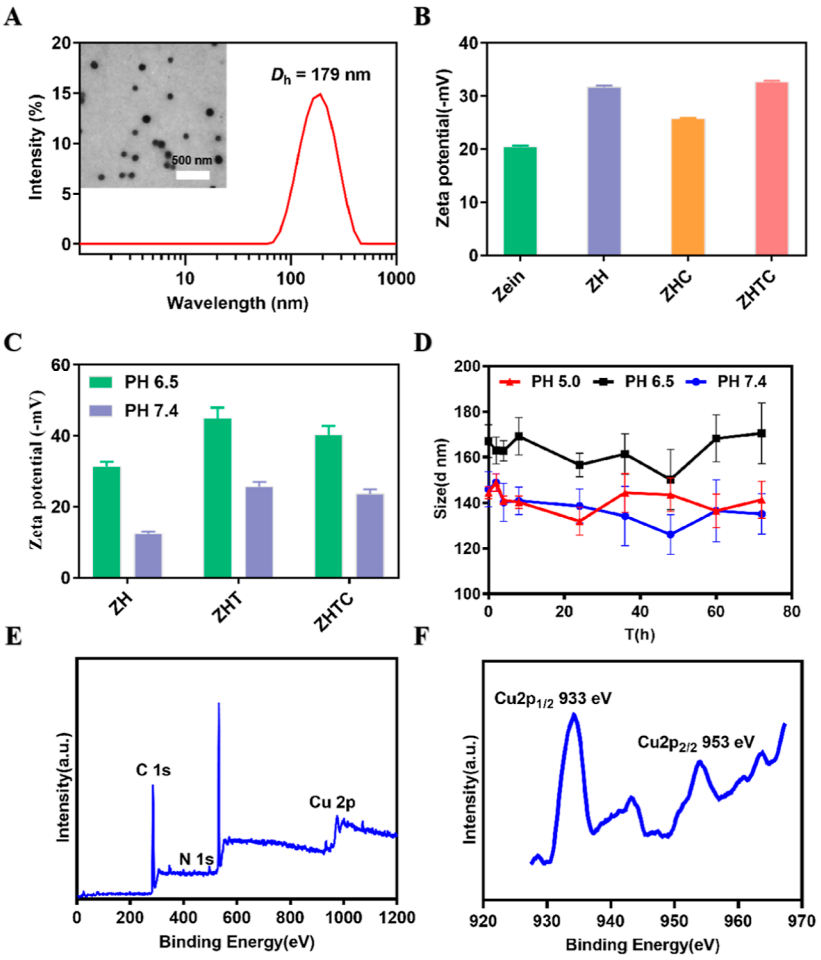

Figure 1. (A) TEM images (inset images) and average particle size of ZHTC@IR780 nanoparticles. (B) Zein, Zein-HA, Zein-HA-Cu, Zein-HA-TA-Cu nanoparticles, and zeta potential. (C) Zein, Zein-HA, Zein-HA-TA, Zein-HA-TA-Cu nanoparticles, and zeta potential under different pH conditions. (D) Storage stability of the ZHTC@IR780 nanoparticles under different pH conditions. (E,F) XPS spectra of ZHTC@IR780 nanoparticles.

After 48 h of incubation, for the MTT assay, the MTT solution (20 μL, 5 mg/mL) was added. After incubation for 4 h, the culture medium was removed. The DMSO solution (150 μL) was added, the plates were subsequently placed on a microplate oscillator for 10 min, and a microplate reader was used to determine the final UV absorbance at a detection wavelength of 490 nm.

In Vitro PDT. CT26 cells were seeded into 24-well plates and then incubated with PBS, IR780, ZH@IR780, ZHT@IR780, and ZHTC@IR780 (IR780 1 μg/mL) at 37 °C under normoxic or hypoxic conditions. The hypoxic condition was achieved by incubating the cells in a hypoxic incubator supplied with a hypoxic gas stream (1% O_2, 5% CO_2, and 94% N_2) for 4 h. Then, the cells were exposed to an 808 nm laser at a power density of 0.1 W cm^{-2} for 60 s. The excess unbound materials were washed three times with PBS. The DCFH-DA (2′,7′-dichlorodihydrofluorescein diacetate) ROS Assay Kit was used to detect the ROS generation inside cells.

Western Blot. CT26 cells were incubated in normoxic or hypoxic conditions. Then, cells were lysed and collected, followed by mixing with sample buffers and heating at 95 °C for 5 min. After electrophoresis with 10% SDS-PAGE (sodium dodecyl sulphate-polyacrylamide gel electrophoresis), proteins were transferred to a polyvinylidene difluoride (PVDF) membrane. The PVDF membrane was stained with primary antibodies against HIF-1α (ab190197, Abcam, Cambridge, MA, USA) to evaluate the degree of hypoxia and against tubulin for the loading control, and then with a horseradish peroxidase (HRP)-labeled secondary antibody. The HIF-1α level was monitored by enhanced chemiluminescence using the Gel Doc system (BioRad).

Immunofluorescence for Cellular Hypoxia. The procedure for CT26 cell culture is the same as that for the western blot. Following different treatments, cells were fixed with 4% paraformaldehyde (PFA) at 37 °C for 20 min and permeabilized with PBS containing 0.2% Triton X-100 at 37 °C for 1 min. After blocking with PBS containing 0.05% Tween-20 buffer and 5% bovine serum albumin (Sigma) at room temperature for 120 min, the cells were incubated with primary antibodies against HIF-1α or calreticulin or PD-L1 in a humidified chamber at room temperature for 120 min, followed by phalloidin (Rhodamine Conjugate) at room temperature for 2 h. Images were captured by DeltaVision SoftWoRx Software (Applied Precision) and processed by deconvolution and z-stack projection.

RESULTS AND DISCUSSION

ZHTC@IR780 NPs Preparation and Characterization. Zein's self-assembly ability, driven by hydrophobicity and hydrophilicity, has been used as a carrier for encapsulation and

https://doi.org/10.1021/acsomega.2c03404
ACS Omega 2022, 7, 29256−29265

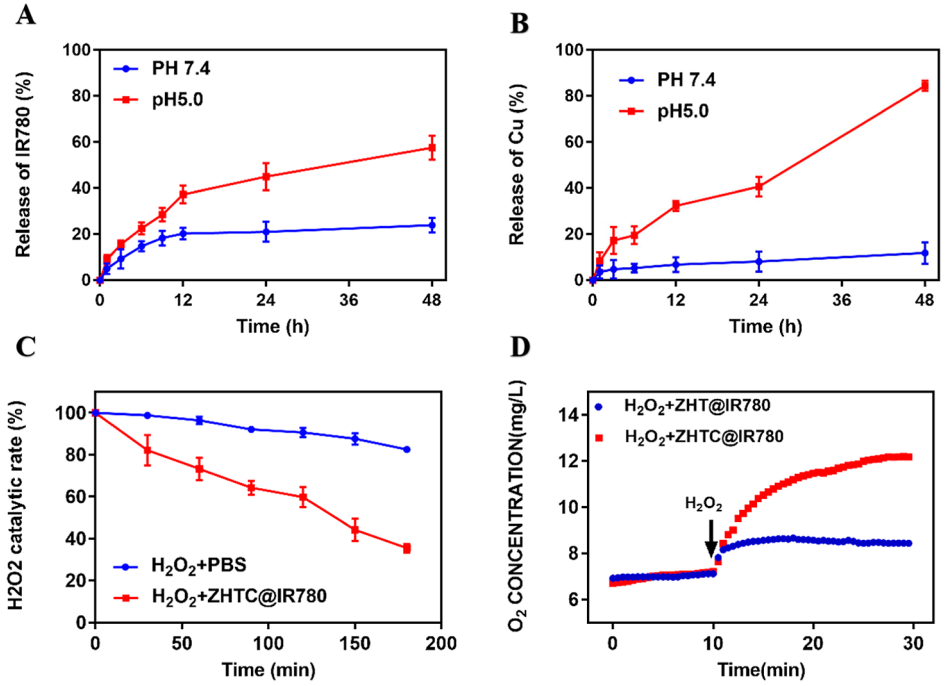

Figure 2. (A) Release profile of IR780 from nanoparticles under different pH conditions. (B) Release profile of Cu^{2+} from nanoparticles under different pH conditions. (C) Catalytic efficiency of ZHTC@IR780 nanoparticles on H_2O_2. (D) Catalysis of H_2O_2 by ZHT@IR780 and ZHTC@IR780 nanoparticles.

controlled release of fat-soluble compounds using a simple antisolvent precipitation method.[33,34] For a brief moment, zein solution and IR780 solution were dripped into HA solution at the same time. Then, in order to stabilize the nanoparticles and achieve the synergistic therapy of chemo-dynamic therapy and photodynamic therapy, tannic acid and copper dichloride solutions were added drop by drop, respectively. Finally, the organic solvent was removed by dialysis and ZHTC@IR780 nanoparticles were obtained.

The surface morphology of the Zein, Zein-HA, Zein-HA-TA-Cu, and ZHTC@IR780 nanoparticles was monitored by TEM. As shown in Figure S1, the nanoparticles prepared with only Zein components showed aggregation and poor dispersion. When hyaluronic acid was added, the dispersion of the nanoparticles was improved. After the addition of tannic acid, metal ion copper, and photosensitizer IR780 iodide, the size and dispersion of the nanoparticles did not change significantly, and they still maintained a uniform spherical structure (Figure 1A). As determined by dynamic light scattering (DLS) (Figure 1A), the average size of fabricated ZHTC@IR780 NPs was approximately 179 nm. In addition, the effect of nanoparticle components was investigated by the zeta potential of nanoparticles. As shown in Figure 1B, when sodium hyaluronate and tannic acid were added, the absolute value of nanoparticle potential was greater than 30, indicating that sodium hyaluronate can increase nanoparticle stability. Furthermore, the potential values of nanoparticles under different pH conditions were detected. The results showed that the potentials of nanoparticles were negative under pH 7.4 and pH 6.5, indicating that they could circulate normally in vivo and meet the requirements of intravenous injection (Figure 1C). The size of ZHTC@IR780 NPs stored at different pH values remained almost unchanged in 72 h, indicating the good stability of ZHTC@IR780 NPs in solution (Figure 1D). X-ray photoelectron spectroscopy (XPS) analysis of ZHTC@IR780 NPs revealed that the Cu existed primarily in the form of Cu^{2+} (Figure 1E,F).

pH-Responsive Release of Drug-Loaded Nanoparticles IR780 and Cu^{2+} In Vitro. Next, we investigated the release of IR780 and Cu^{2+} by ZHTC@IR780 nanoparticles in the blood circulation microenvironment (pH 7.4) and in the lysosomal microenvironment (pH 5.0) using dialysis. As shown in Figure 2A,B, only slow release of IR780 (less than 24%) and Cu^{2+} (12%) from NPs was observed at pH 7.4 after 48 h of incubation. By contrast, after 48 h of incubation at pH 5, approximately 57% of IR780 and 84% of Cu^{2+} were released into the medium. The results showed that ZHTC@IR780 nanoparticles had good stability and would not cause systemic toxicity caused by a large amount of drug released into the blood circulation. It also indicated that the nanoparticles had good pH response and release characteristics.

Photodynamic Chemical Dynamics Detection at the Solution Level. The catalytic ability of nanoparticles to H_2O_2 was determined using an H_2O_2 kit. As shown in Figure 2C, the catalytic efficiency of ZHTC@IR780 after 180 min reached 64.58%, which was 47% higher than that of natural decomposition at 17.58%, indicating that ZHTC@IR780 nanoparticles had a good ability to catalyze H_2O_2. Furthermore, by detecting the change of oxygen content in the solution after the addition of ZHTC@IR780, adding H_2O_2 at the 10th minute, and comparing it to the PBS group without copper ions, Figure 2D shows that ZHTC@IR780 nanoparticles could significantly improve the decomposition of H_2O_2 to O_2, while the catalytic efficiency of the control group was average. These experimental results indicate that ZHTC@IR780 NPs could accelerate H_2O_2 decomposition to generate O_2, which might alleviate tumor hypoxia and provide necessary conditions for photodynamic therapy.

Under the catalysis of ferrous ions (Fe^{2+}) or other Fenton-like ions,[35−38] Fenton or Fenton-like reactions can generate

https://doi.org/10.1021/acsomega.2c03404
ACS Omega 2022, 7, 29256−29265

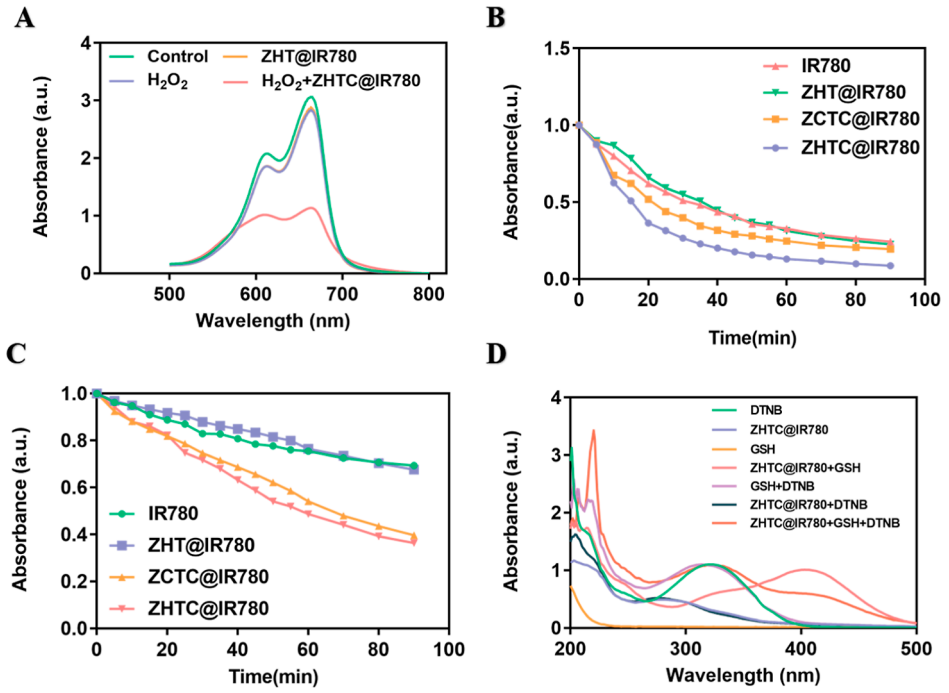

Figure 3. (A) UV−vis absorption curves of MB solution after different treatments. (B) In vitro $^1O_2$ assay under anaerobic conditions, the relative absorbance of DPBF at 410 nm in the solution changes with time. (C) In vitro $^1O_2$ assay under aerobic conditions, the relative absorbance of DPBF at 410 nm in the solution changes with time. (D) Oxidative glutathione-like catalysis of ZHTC@IR780 nanoparticles.

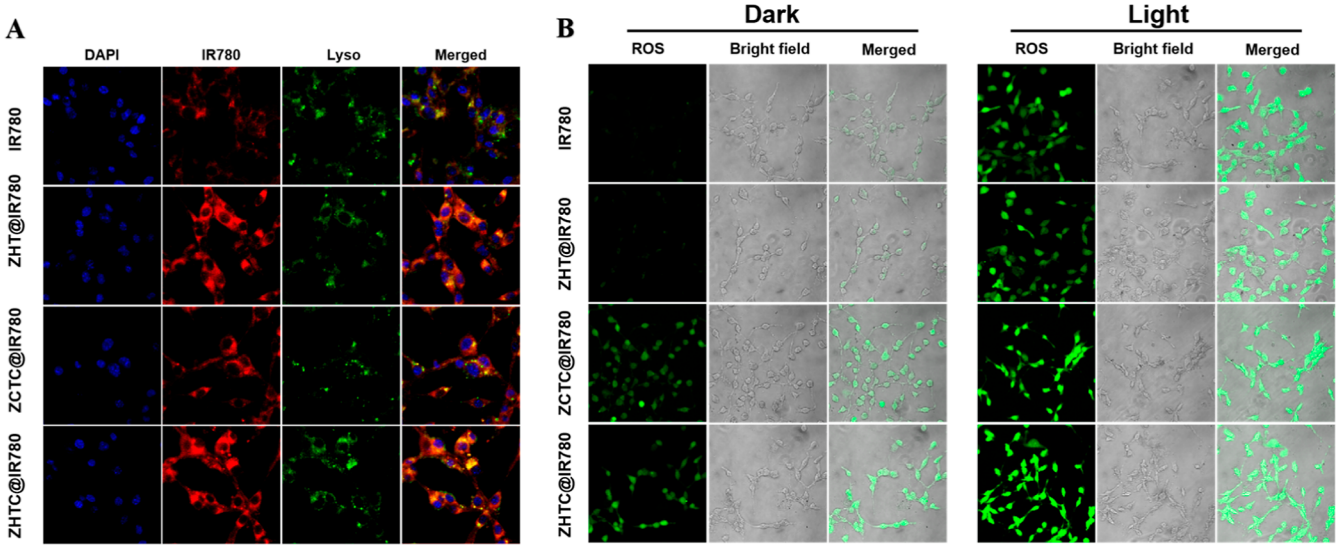

Figure 4. (A) CLSM image of CT26 cells after 4 h of co-culture with IR780, ZHT@IR780, ZCTC@IR780, and ZHTC@IR780. From left to right in each column are the DAPI fluorescence of the nucleus, IR780 fluorescence, Lyso-Tracker fluorescence of the lysosome, and the superposition of all fluorescence. (B) CLSM observation of CT26 cells' uptake of small molecules IR780, ZHT@IR780, ZCTC@IR780, and ZHTC@IR780 and the dark control group's and light experimental group's ROS production.

oxidative $^{\bullet}OH$ from H_2O_2. CDT can alleviate the oxygen deficiency in PDT and improve its therapeutic effect. The generated O_2 can increase the production efficiency of $^{\bullet}OH$ through near-infrared laser irradiation, thereby enhancing the antitumor effect of CDT. The Cu of ZHTC@IR780 nanoparticles could result in a Fenton-like reaction, catalyzing H_2O_2 to produce O_2 and $^{\bullet}OH$. Furthermore, $^{\bullet}OH$ could degrade methylene blue (MB), and the production of $^{\bullet}OH$ can be detected by the change of methylene blue ultraviolet absorption. In Figure 3A, the MB degradation capacity of the ZHTC@IR780 nanoparticles group with additional H_2O_2 was assayed, which was obviously elevated due to more $^{\bullet}OH$ generation. As shown in Figure S2, with the extension of time, the absorption peak of methylene blue was getting lower and lower, indicating that $^{\bullet}OH$ can be continuously produced to degrade MB. The results showed that the nanoparticle had good chemical kinetic activity in vitro.

The generated $^1O_2$ from an NIR-irradiated ZHTC@IR780 nanoparticles solution without and with O_2 was measured by the degradation experiments of the 1,3-diphenylisobenzofuran (DPBF) reagent. With the accumulation of light time, the absorption value of the ZHTC@IR780 + DPBF solution at

https://doi.org/10.1021/acsomega.2c03404
ACS Omega 2022, 7, 29256−29265

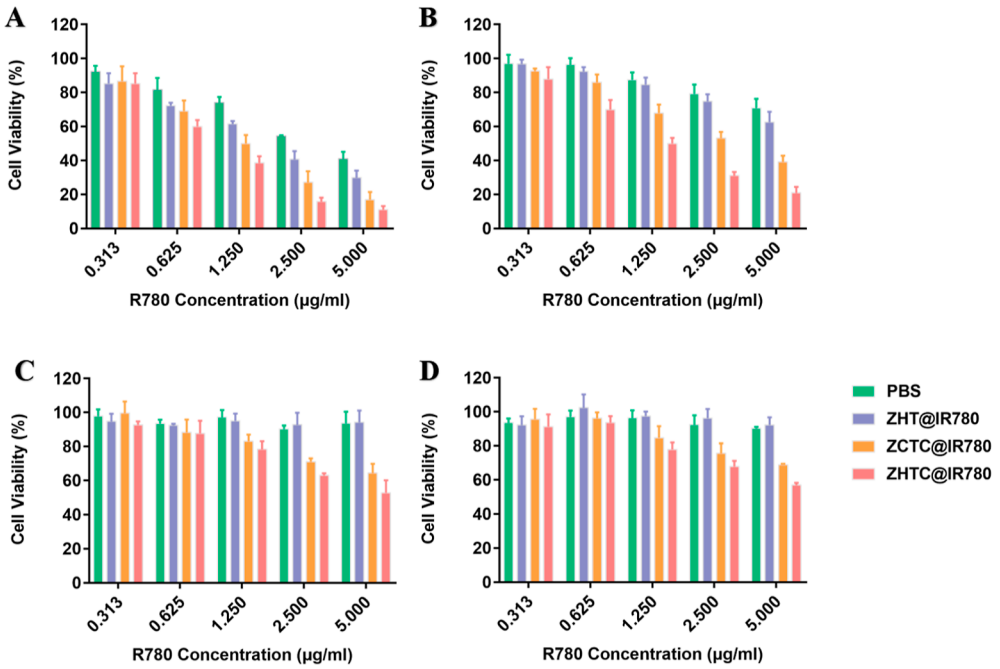

Figure 5. CT26 cell pairs ZHT@IR780, ZCTC@IR780, and ZHTC@IR780 in light cell survival rate after 48 h of treatment at 37 °C with aerobic (A), nonlight and aerobic (B), light and anaerobic (C), and nonlight and anaerobic (D) treatments.

410 nm decreased the most (91.65%), which was significantly faster than the other three groups of solutions (Figures 3B and S3A). It indicated the $^1O_2$ production efficacy of the ZHTC@IR780 nanoparticles solution was greatly improved due to more O_2 supplementation caused by the Fenton reaction. ZHTC@IR780 NPs had the function of catalytic enzymes like H_2O_z to catalyze H_2O_2 to continuously supplement oxygen in solution, which promoted the production of $^1O_2$. With the NIR-irradiated ZHTC@IR780 deaeration group as the control, Figures 3C and S4A showed that the absorbance drop of DPBF at 410 nm (62.78%) was much smaller than that of the no deaeration group. At the same time, compared to other controls, the ZHTC@IR780 nanoparticle solution had the best effect on $^1O_2$ production.

Next, we studied the role of ZHTC@IR780 nanoparticles in the elimination of glutathione in vitro. Using 5,5′-dithiobis-(2-nitrobenzoic acid) (DTNB) as an indicator, GSH could react with it to form yellow 5-thio-2-nitrobenzoic acid. As can be seen from Figure 3D, DTNB had an obvious absorption peak at 323 nm. After GSH was added, the peak at 323 nm was significantly weakened, and a new peak appeared at 408 nm, indicating the formation of 5-thio-2-nitrobenzoic acid. However, if GSH first reacted with ZHTC@IR780 nanoparticles for 10 min, it was found that GSH did not react with DTNB, indicating that GSH was consumed by ZHTC@IR780 nanoparticles. In addition, it was verified through experiments that ZHTC@IR780 nanoparticles did not interact with DTNB. Based on all the abovementioned results, it is proved that the ZHTC@IR780 nanoparticles also exhibited excellent GSH depletion properties.

In Vitro Cellular Uptake of NPs and Production of ROS. The content of photosensitizers in cells is one of the important factors that determine the effect of photodynamic therapy. The more drugs that are endocytosed by cells, the more ROS will be produced under light conditions. First, the amount of free IR780, ZHT@IR780, ZCTC@IR780, and ZHTC@IR780 NPs internalized by CT26 cells was investigated qualitatively by confocal microscopy. As shown in Figure 4A, a very weak fluorescence signal was observed after cell incubation with free IR780 for 4 h, suggesting that the free IR780 failed to efficiently enter CT26 cells. The endocytosis of small molecular IR780 was significantly less than that of drug-loaded nanoparticles. Furthermore, the endocytosis of ZCTC@IR780 was lower than that of ZHT@IR780 and ZHTC@IR780 due to the presence of hyaluronic acid, which could target the cellular protein CD44 and increase the endocytosis of nanoparticles.[39−41] However, the endocytosis of ZHT@IR780 and ZHTC@IR780 was basically the same. This indicated that the ZHTC@IR780 possessed a good active-targeting ability to enhance NP accumulation in the tumor.

In the abovementioned processes, both H_2O_2 and GSH play important roles in yielding $^1O_2$ and $^{\bullet}OH$, and the GSH depletion is also good for the existence of ROS. The ZHTC@IR780 NPs-mediated ROS (including both $^1O_2$ and $^{\bullet}OH$) generation in CT26 cancer cells was tested with the intracellular 2,7-dichlorofluorescin diacetate (DCFH-DA) probe to radiate green fluorescence with the oxidation state. In Figure 4B, compared with the other control groups, CT26 cells incubated with ZHTC@IR780 nanoparticles posed stronger green fluorescence, while ZHTC@IR780 and NIR-treated cells posed the strongest signal due to the increased amount of ROS from the combined PDT and CDT effects. However, the green fluorescence of ZCTC@IR780 was relatively weak, which proved that ZHTC@IR780 had a targeted function. In addition, the green fluorescence of ZHT@IR780 was not as good as that of ZHTC@IR780. This is because the Fenton-like reaction could not take place, and only small amounts of ROS were generated. Also, the green fluorescence was the weakest in the small molecular IR780 group.

In Vitro Cytotoxicity Research. To evaluate the cytotoxicity of ZHTC@IR780 NPs, we next used an MTT assay to analyze CT26 cells. As shown in Figure 5, the cell viability of the irradiated and aerobic groups decreased rapidly

https://doi.org/10.1021/acsomega.2c03404
ACS Omega 2022, 7, 29256−29265

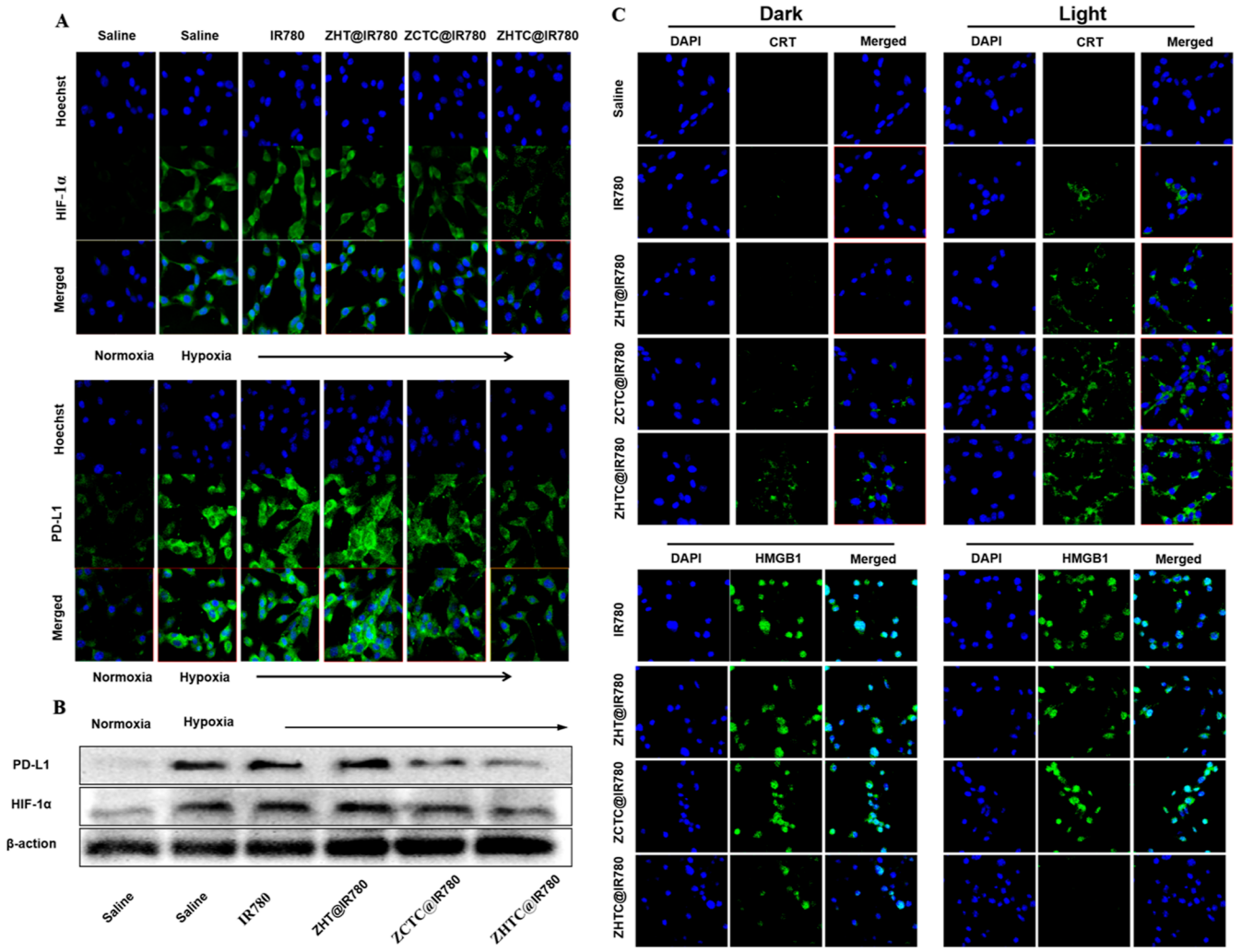

Figure 6. (A) CLSM observation of CT26 cells' uptake of small molecules IR780, ZHT@IR780, ZCTC@IR780, and ZHTC@IR780 and changes in intracellular PD-L1 and HIF-1α. (B) Western blot analysis of the changes in PD-L1 and HIF-1 expression levels of different treatments. (C) CLSM-measured calcium reticulin outgrowth and HMGB1 content in the nucleus of CT26 cells after uptake of small molecules IR780, ZHT@IR780, ZCTC@IR780, and ZHTC@IR780 under dark and light conditions.

when the concentration of IR780 increased, demonstrating the concentration-dependent cytotoxicity of IR780-based preparations. Furthermore, ZHTC@IR780 exhibited obvious photodynamic cytotoxicity to CT26 cells, which was greater than that of the IR780, ZHT@IR780, and ZCTC@IR780 groups. The half-maximal inhibitory concentration (IC_{50}) in the light and aerobic ZHTC@IR780 groups was 0.8864 μg/mL for IR780, much lower than that of other groups. However, the anaerobic group did not reach the half-maximal inhibitory dose regardless of the 808 nm laser.

HIF-1α and PD-L1 Expression in Tumor Cells following Treatment with ZHTC@IR780 NPs. The effective relief of tumor hypoxia was also confirmed by measuring the expression of HIF-1α.[42] According to the in vitro results, ZHTC@IR780-triggered generation of O_2 with H_2O_2 after laser irradiation might be helpful to relieve tumor hypoxia. Results as shown in Figure 6A, through Western blot analysis, could be seen that the expression of the ZHTC@IR780 group was the least, which was consistent with the result of CLSM. The relief of tumor hypoxia is a key factor in improving the therapeutic efficiency of PDT and inhibiting tumor metastasis.

PD-L1 is highly expressed on the surface of tumor cells. The purpose of this study was to investigate the effect of improving tumor hypoxia on the expression of PD-L1. From Figure 6B, it could be seen that under normal oxygen conditions, tumor cells in the normal saline group expressed a certain amount of PD-L1, and under hypoxia conditions, saline, small molecular IR780, and ZHT@IR780 tumor cells highly expressed PD-L1. Although the ZCTC@IR780 group can produce a Fenton-like reaction and relieve hypoxia in tumor cells, the effect is generally owing to the small amount of endocytosis. Compared with cells cultured under other hypoxia conditions, the expression of PD-L1 in the cells co-incubated with ZHTC@IR780 was low, indicating that it could alleviate the hypoxia state of tumor cells. In addition, Western blot results showed that the expression level of the ZHTC@IR780 group was the lowest, which was in accordance with that of CLSM (Figure 6B).

Effect of PDT-Induced ICD. We tried to investigate the effect of photodynamic therapy (PDT)-induced ICD by measuring the expression of calreticulin (CRT) and the release of high mobility histone 1 (HMGB1). CLSM results showed that only a little induced CRT was exposed to the surface of

https://doi.org/10.1021/acsomega.2c03404
ACS Omega 2022, 7, 29256−29265

CT26 cells in the unirradiated group. On the contrary, the combination of ZCTC@IR780 and ZHTC@IR780 with laser irradiation significantly promoted the expression of CRT (Figure 6C).

HMGB1 is a known danger signal that stimulates DC to engulf dying tumor cells. Figure 6C showed that HMGB1 was mainly located in the nucleus of CT26 incubated with saline, ZHT@IR780, and ZCTC@IR780. Both PDT in the ZHT@IR780 + L and ZCTC@IR780 + L groups could induce the moderate release of HMGB1. In contrast, HMGB1 was almost completely released from the nucleus in the ZHTC@IR780 group. In conclusion, the data from CRT exposure and HMGB1 release secretion confirmed the accumulation of ICD induced by ZHTC@IR780-based PDT in vitro.

CONCLUSIONS

In summary, zein, a natural protein of plant origin, has greater advantages over other synthetic polymers used in controlled drug and biomedical delivery systems due to its safety and biocompatibility. Here, we fabricated multifunctional nanoparticles using zein/hyaluronate acid (HA)/tannin (TA)/Cu^{2+} loading them with IR780 (ZHTC@IR780), which has high tumor cell targeting and catalytic action of catalase (CAT)-like and glutathione peroxidase-like activities. In addition, Zein-HA-TA-Cu@IR780 nanoparticles have good photodynamic and chemical kinetic effects and can undergo Fenton-like reactions to catalyze the production of cytotoxic hydroxyl radicals ($^{\bullet}OH$) from H_2O_2 as well as the production of single-linear oxygen ($^1O_2$) by near-infrared light. 808 nm laser irradiation can produce singlet oxygen ($^1O_2$). The good photodynamic and the chemical kinetic effects of Zein-HA-TA-Cu@IR780 nanoparticles were verified at the nanoparticle aqueous solution level as well as at the cellular level. The endocytosis assay of nanoparticles by cells observed by laser confocal microscopy showed that Zein-HA-TA-Cu@IR780 nanoparticles were mostly taken up by cells, which verified that Zein-HA-TA-Cu@IR780 nanoparticles have a targeting function. However, this research is to investigate the killing effect on mouse colorectal cancer cells and its mechanism at the cellular level. Further research is needed on the antitumor effect at the animal level.

ASSOCIATED CONTENT

Supporting Information

The Supporting Information is available free of charge at https://pubs.acs.org/doi/10.1021/acsomega.2c03404.

TEM images of Zein, Zein-HA, and Zein-HA-TA-Cu; UV−vis absorption curves of MB solutions at different times; and In vitro $^1O_2$ assay under aerobic and anaerobic conditions (PDF)

AUTHOR INFORMATION

Corresponding Authors

Dongfang Zhou − *Guangdong Provincial Key Laboratory of New Drug Screening, School of Pharmaceutical Sciences, Southern Medical University, Guangzhou 510515, China;* orcid.org/0000-0002-8381-7440; Email: dfzhou@smu.edu.cn

Hao Zhang − *College of Food Science and Engineering, National Engineering Laboratory for Wheat and Corn Deep Processing, Jilin Agricultural University, Changchun, Jilin 130118, China*; Phone: +86-43184533321; Email: zhanghao3318@sina.com

Authors

Xiang Li − *College of Food Science and Engineering, National Engineering Laboratory for Wheat and Corn Deep Processing, Jilin Agricultural University, Changchun, Jilin 130118, China*

Yupeng Wang − *Guangdong Provincial Key Laboratory of New Drug Screening, School of Pharmaceutical Sciences, Southern Medical University, Guangzhou 510515, China*

Qiankun Shi − *College of Food Science and Engineering, National Engineering Laboratory for Wheat and Corn Deep Processing, Jilin Agricultural University, Changchun, Jilin 130118, China*

Nuo Zhen − *College of Food Science and Engineering, National Engineering Laboratory for Wheat and Corn Deep Processing, Jilin Agricultural University, Changchun, Jilin 130118, China*

Jin Xue − *College of Food Science and Engineering, National Engineering Laboratory for Wheat and Corn Deep Processing, Jilin Agricultural University, Changchun, Jilin 130118, China*

Jingsheng Liu − *College of Food Science and Engineering, National Engineering Laboratory for Wheat and Corn Deep Processing, Jilin Agricultural University, Changchun, Jilin 130118, China*

Complete contact information is available at: https://pubs.acs.org/10.1021/acsomega.2c03404

Notes

The authors declare no competing financial interest.

ACKNOWLEDGMENTS

The authors gratefully acknowledge the financial support provided by the National Natural Science Foundation of China (no. 32072169).

REFERENCES

(1) Song, W.; Kuang, J.; Li, C.-X.; Zhang, M.; Zheng, D.; Zeng, X.; Liu, C.; Zhang, X.-Z. Enhanced Immunotherapy Based on Photodynamic Therapy for Both Primary and Lung Metastasis Tumor Eradication. *ACS Nano* **2018**, *12*, 1978−1989.

(2) Hiller, J. G.; Perry, N. J.; Poulogiannis, G.; Riedel, B.; Sloan, E. K. Perioperative events influence cancer recurrence risk after surgery. *Nat. Clin. Pract. Oncol.* **2018**, *15*, 205−218.

(3) Castle, K. D.; Kirsch, D. G. Establishing the Impact of Vascular Damage on Tumor Response to High-Dose Radiation Therapy. *Cancer Res.* **2019**, *79*, 5685.

(4) Kim, J. J.; Tannock, I. F. Repopulation of cancer cells during therapy: an important cause of treatment failure. *Nat. Rev. Cancer* **2005**, *5*, 516−525.

(5) Zhou, F.; Feng, B.; Yu, H.; Wang, D.; Wang, T.; Ma, Y.; Wang, S.; Li, Y. Tumor Microenvironment-Activatable Prodrug Vesicles for Nanoenabled Cancer Chemoimmunotherapy Combining Immunogenic Cell Death Induction and CD47 Blockade. *Adv. Mater.* **2019**, *31*, 1805888.

(6) Wang, H.; Han, X.; Dong, Z.; Xu, J.; Wang, J.; Liu, Z. Hyaluronidase with pH-responsive Dextran Modification as an Adjuvant Nanomedicine for Enhanced Photodynamic-Immunotherapy of Cancer. *Adv. Funct. Mater.* **2019**, *29*, 1902440.

(7) Meng, Z.; Zhou, X.; Xu, J.; Han, X.; Dong, Z.; Wang, H.; Zhang, Y.; She, J.; Xu, L.; Wang, C.; Liu, Z. Light-Triggered In Situ Gelation to Enable Robust Photodynamic-Immunotherapy by Repeated Stimulations. *Adv. Mater.* **2019**, *31*, 1900927.

(8) An, J.; Zhu, L.; Wang, N.; Song, Z.; Yang, Z.; Du, D. H.; Tang, H. Photo-Fenton like degradation of tetrabromobisphenol A with

grapheneBiFeO3 composite as a catalyst. *Chem. Eng. J.* **2013**, *219*, 225−237.
(9) Tian, Q.; Li, Y.; Jiang, S.; An, L.; Lin, J.; Wu, H.; Huang, P.; Yang, S. Tumor pH-Responsive Albumin/Polyaniline Assemblies for Amplified Photoacoustic Imaging and Augmented Photothermal Therapy. *Small* **2019**, *15*, 1902926.
(10) Fan, W.; Huang, P.; Chen, X. Overcoming the Achilles' heel of photodynamic therapy. *Chem. Soc. Rev.* **2016**, *45*, 6488−6519.
(11) Zhou, Z.; Song, J.; Nie, L.; Chen, X. Reactive oxygen species generating systems meeting challenges of photodynamic cancer therapy. *Chem. Soc. Rev.* **2016**, *45*, 6597−6626.
(12) Zhang, Y.; Cheng, Y.; Yang, F.; Yuan, Z.; Wei, W.; Lu, H.; Dong, H.; Zhang, X. Near-infrared triggered Ti3C2/g-C3N4 heterostructure for mitochondria-targeting multimode photodynamic therapy combined photothermal therapy. *Nano Today* **2020**, *34*, 100919.
(13) Park, H.; Kim, J.; Jung, S.; Kim, W. J. DNA-Au Nanomachine Equipped with i-Motif and G-Quadruplex for Triple Combinatorial Anti-Tumor Therapy. *Adv. Funct. Mater.* **2018**, *28*, 1705416.
(14) Feng, L.; Cheng, L.; Dong, Z.; Tao, D.; Barnhart, T. E.; Cai, W.; Chen, M.; Liu, Z. Theranostic Liposomes with Hypoxia-Activated Prodrug to Effectively Destruct Hypoxic Tumors Post-Photodynamic Therapy. *ACS Nano* **2017**, *11*, 927−937.
(15) Hu, J.-J.; Lei, Q.; Zhang, X.-Z. Recent advances in photonanomedicines for enhanced cancer photodynamic therapy. *Prog. Mater. Sci.* **2020**, *114*, 100685.
(16) Jia, T.; Wang, Z.; Sun, Q.; Dong, S.; Xu, J.; Zhang, F.; Feng, L.; He, F.; Yang, D.; Yang, P.; Lin, J. Intelligent Fe−Mn Layered Double Hydroxides Nanosheets Anchored with Upconversion Nanoparticles for Oxygen-Elevated Synergetic Therapy and Bioimaging. *Small* **2020**, *16*, 2001343.
(17) Xu, J.; Gulzar, A.; Liu, Y.; Bi, H.; Gai, S.; Liu, B.; Yang, D.; He, F.; Yang, P. Integration of IR-808 Sensitized Upconversion Nanostructure and MoS2 Nanosheet for 808 nm NIR Light Triggered Phototherapy and Bioimaging. *Small* **2017**, *13*, 1701841.
(18) Feng, B.; Hou, B.; Xu, Z.; Saeed, M.; Yu, H.; Li, Y. Self-Amplified Drug Delivery with Light-Inducible Nanocargoes to Enhance Cancer Immunotherapy. *Adv. Mater.* **2019**, *31*, 1902960.
(19) Chang, M.; Wang, M.; Wang, M.; Shu, M.; Ding, B.; Li, C.; Pang, M.; Cui, S.; Hou, Z.; Lin, J. A Multifunctional Cascade Bioreactor Based on Hollow-Structured Cu2MoS4 for Synergetic Cancer Chemo-Dynamic Therapy/Starvation Therapy/Phototherapy/Immunotherapy with Remarkably Enhanced Efficacy. *Adv. Mater.* **2019**, *31*, 1905271.
(20) Fan, J.-X.; Peng, M.-Y.; Wang, H.; Zheng, H.-R.; Liu, Z.-L.; Li, C.-X.; Wang, X.-N.; Liu, X.-H.; Cheng, S.-X.; Zhang, X.-Z. Engineered Bacterial Bioreactor for Tumor Therapy via Fenton-Like Reaction with Localized H_2O_2 Generation. *Adv. Mater.* **2019**, *31*, 1808278.
(21) Zhao, Z.; Wang, W.; Li, C.; Zhang, Y.; Yu, T.; Wu, R.; Zhao, J.; Liu, Z.; Liu, J.; Yu, H. Reactive Oxygen Species−Activatable Liposomes Regulating Hypoxic Tumor Microenvironment for Synergistic Photo/Chemodynamic Therapies. *Adv. Funct. Mater.* **2019**, *29*, 1905013.
(22) Tang, Z.; Liu, Y.; He, M.; Bu, W. Chemodynamic Therapy: Tumour Microenvironment-Mediated Fenton and Fenton-like Reactions. *Angew. Chem., Int. Ed.* **2019**, *58*, 946−956.
(23) Ku, T.; Gill, S.; Löbenberg, R.; Azarmi, S.; Roa, W.; Prenner, E. J. Size dependent interactions of nanoparticles with lung surfactant model systems and the significant impact on surface potential. *J. Nanosci. Nanotechnol.* **2008**, *8*, 2971−2978.
(24) Wang, X.; Fan, Y.; Yan, J.; Yang, M. Engineering polyphenol-based polymeric nanoparticles for drug delivery and bioimaging. *Chem. Eng. J.* **2022**, *439*, 135661.
(25) Weissmueller, N. T.; Lu, H. D.; Hurley, A.; Prud'homme, R. K. Nanocarriers from GRAS zein proteins to encapsulate hydrophobic actives. *Biomacromolecules* **2016**, *17*, 3828−3837.
(26) Wang, Y.; Padua, G. W. Formation of Zein Microphases in Ethanol−Water. *Langmuir* **2010**, *26*, 12897−12901.
(27) Anirudhan, T.; Varghese, S.; Manjusha, V. Hyaluronic acid coated Pluronic F127/Pluronic P123 mixed micelle for targeted delivery of Paclitaxel and Curcumin. *Int. J. Biol. Macromol.* **2021**, *192*, 950−957.
(28) Zhang, Q.; Wang, J.; Liu, D.; Zhu, W.; Guan, S.; Fan, L.; Cai, D. Targeted delivery of honokiol by zein/hyaluronic acid core-shell nanoparticles to suppress breast cancer growth and metastasis. *Carbohydr. Polym.* **2020**, *240*, 116325.
(29) Bigham, A.; Rahimkhoei, V.; Abasian, P.; Delfi, M.; Naderi, J.; Ghomi, M.; Moghaddam, F. D.; Waqar, T.; Ertas, Y. N.; Sharifi, S. Advances in tannic acid-incorporated biomaterials: Infection treatment, regenerative medicine, cancer therapy, and biosensing. *Chem. Eng. J.* **2022**, *432*, 134146.
(30) Song, B.; Yang, L.; Han, L.; Jia, L. Metal ion-chelated tannic acid coating for hemostatic dressing. *Materials* **2019**, *12*, 1803.
(31) Jöbstl, E.; OConnell, J.; Fairclough, J. P. A.; Williamson, M. P. Molecular model for astringency produced by polyphenol/protein interactions. *Biomacromolecules* **2004**, *5*, 942−949.
(32) Deng, Z.; Wang, S.; Pei, Y.; Zhou, B.; Li, J.; Hou, X.; Li, B.; Liang, H. Tuning of molecular Interactions between zein and tannic acid to modify sunflower sporopollenin exine capsules: enhanced stability and targeted delivery of bioactive macromolecules. *ACS Appl. Bio Mater.* **2021**, *4*, 2686−2695.
(33) Huang, X.; Liu, Y.; Zou, Y.; Liang, X.; Peng, Y.; McClements, D. J.; Hu, K. Encapsulation of resveratrol in zein/pectin core-shell nanoparticles: Stability, bioaccessibility, and antioxidant capacity after simulated gastrointestinal digestion. *Food Hydrocolloids* **2019**, *93*, 261−269.
(34) Kaushik, P.; Priyadarshini, E.; Rawat, K.; Rajamani, P.; Bohidar, H. B. pH responsive doxorubucin loaded zein nanoparticle cross-linked pectin hydrogel as effective site-specific anticancer substrates. *Int. J. Biol. Macromol.* **2020**, *152*, 1027−1037.
(35) Zheng, D.-W.; Lei, Q.; Zhu, J.-Y.; Fan, J.-X.; Li, C.-X.; Li, C.; Xu, Z.; Cheng, S.-X.; Zhang, X.-Z. Switching Apoptosis to Ferroptosis: Metal−Organic Network for High-Efficiency Anticancer Therapy. *Nano Lett.* **2017**, *17*, 284−291.
(36) Tang, Z.; Zhang, H.; Liu, Y.; Ni, D.; Zhang, H.; Zhang, J.; Yao, Z.; He, M.; Shi, J.; Bu, W. Antiferromagnetic Pyrite as the Tumor Microenvironment-Mediated Nanoplatform for Self-Enhanced Tumor Imaging and Therapy. *Adv. Mater.* **2017**, *29*, 1701683.
(37) Liu, Y.; Zhen, W.; Jin, L.; Zhang, S.; Sun, G.; Zhang, T.; Xu, X.; Song, S.; Wang, Y.; Liu, J.; Zhang, H. All-in-One Theranostic Nanoagent with Enhanced Reactive Oxygen Species Generation and Modulating Tumor Microenvironment Ability for Effective Tumor Eradication. *ACS Nano* **2018**, *12*, 4886−4893.
(38) Liu, Y.; Zhen, W.; Wang, Y.; Liu, J.; Jin, L.; Zhang, T.; Zhang, S.; Zhao, Y.; Song, S.; Li, C.; Zhu, J.; Yang, Y.; Zhang, H. One-Dimensional Fe2P Acts as a Fenton Agent in Response to NIR II Light and Ultrasound for Deep Tumor Synergetic Theranostics. *Angew. Chem., Int. Ed.* **2019**, *58*, 2407−2412.
(39) Gong, T.; Dong, Z.; Fu, Y.; Gong, T.; Deng, L.; Zhang, Z. Hyaluronic acid modified doxorubicin loaded Fe3O4 nanoparticles effectively inhibit breast cancer metastasis. *J. Mater. Chem. B.* **2019**, *7*, 5861−5872.
(40) Huang, W.-C.; Chen, S.-H.; Chiang, W.-H.; Huang, C.-W.; Lo, C.-L.; Chern, C.-S.; Chiu, H.-C. Tumor Microenvironment-Responsive Nanoparticle Delivery of Chemotherapy for Enhanced Selective Cellular Uptake and Transportation within Tumor. *Biomacromolecules* **2016**, *17*, 3883−3892.
(41) Ravar, F.; Saadat, E.; Gholami, M.; Dehghankelishadi, P.; Mahdavi, M.; Azami, S.; Dorkoosh, F. A. Hyaluronic acid-coated liposomes for targeted delivery of paclitaxel, in-vitro characterization and in-vivo evaluation. *J. Controlled Release* **2016**, *229*, 10−22.
(42) Deng, Y.; Song, P.; Chen, X.; Huang, Y.; Hong, L.; Jin, Q.; Ji, J. 3-Bromopyruvate-Conjugated Nanoplatform-Induced Pro-Death Autophagy for Enhanced Photodynamic Therapy against Hypoxic Tumor. *ACS Nano* **2020**, *14*, 9711−9727.

https://doi.org/10.1021/acsomega.2c03404
ACS Omega 2022, 7, 29256−29265